Available online at www.sciencedirect.com

SciVerse ScienceDirect

Ceramics International 39 (2013) 3103–3111

CERAMICS INTERNATIONAL

www.elsevier.com/locate/ceramint

High-temperature mechanical properties of reduced NiO–8YSZ anode-supported bi-layer SOFC structures in ambient air and reducing environments

Somnath Biswas[a], Thangamani Nithyanantham[b], Saraswathi Nambiappan Thangavel[c], Sukumar Bandopadhyay[d,*]

[a]*The LNM Institute of Information Technology, Jaipur-302031, India*
[b]*School of Chemical and Biotechnology, Sastra University, Thanjavur-613401, India*
[c]*Department of Bioinformatics, Sastra University, Thanjavur-613401, India*
[d]*College of Engineering and Mines, University of Alaska Fairbanks, AK 99775, USA*

Received 1 August 2012; received in revised form 25 September 2012; accepted 26 September 2012
Available online 7 October 2012

Abstract

This paper describes a study of the mechanical properties of the bi-layer half-cell structures of solid oxide fuel cells (SOFCs) at elevated temperatures in both ambient air and reducing environments. Half-cells with a thin, dense electrolyte layer of 8YSZ, supported by a thick, porous NiO–8YSZ anode precursor structure, were reduced in a gas mixture of 5% H_2–95% Ar at 800 °C for selected time periods of up to 8 h. The development of the essential porous microstructure when forming the Ni–8YSZ anode cermet phase and its resulting effects on the equibiaxial strength, hardness and elastic properties of the half-cell structure were investigated in detail. Two sets of samples with different anode thicknesses were studied simultaneously to determine the effects of anode thickness on the SOFC structure's mechanical properties. The results were analyzed in relation to the porosity and composition of the samples.

Keywords: B. Porosity; C. Mechanical properties; E. Fuel cells; NiO–8YSZ

1. Introduction

The mechanical endurance of ceramic component layers at high operating temperatures in reactive fuel environments is extremely important to ensuring the reliability of SOFCs and similar devices based on dense ion-conducting ceramic membranes [1–5]. Various challenges are inherent to these devices due to their high operating temperatures and multilayered laminate structures, including mechanical and thermal stresses during fabrication and stack assembly and their extensive servicing periods. Much of the degrading force originates from a mismatch in the thermo-mechanical stresses of the different layers, which arises primarily from a disparity in the coefficient of thermal expansion (CTE) in successive layers and depends on the effective Young's modulus of the multilayered structure [6–8]. Mismatched stresses can result in the delamination of layers or the formation of micro-cracks in the layers or interfaces.

To withstand the mechanical effects and maintain the structural integrity of the SOFC stack, at least one of the SOFC components must have an adequate thickness and be mechanically robust to provide structural support to the cell. The electrolyte is kept as thin as possible in an anode-supported SOFC, which is supposed to an improvement over the electrolyte-supported SOFC, to decrease ohmic losses through the electrolyte and lower the operating temperature of the cell. Hence, the cathode remains a weak and compliant material [4,7–10], and the anode or anode-supported electrolyte (half-cell structure) in this type of design becomes solely responsible for the structural integrity and reliability of the cell [8,11,12].

Porous cermets of Ni–YSZ, often fabricated by reducing a NiO–YSZ precursor structure, are preferred anode materials

*Corresponding author.
E-mail address: sbandopadhyay@alaska.edu (S. Bandopadhyay).

0272-8842/$ - see front matter © 2012 Elsevier Ltd and Techna Group S.r.l. All rights reserved.
http://dx.doi.org/10.1016/j.ceramint.2012.09.090

for SOFCs in both tubular- and planar-type designs. Ni–YSZ is favored for its enviable properties, including excellent electro-catalytic activity for H_2 oxidation reactions at the triple phase boundary (TPB) among Ni, YSZ, and gaseous H_2 [13–15]; its high electronic and ionic conductivity [16]; and its structural stability at high operating temperatures in reducing atmosphere [3,16]. Moreover, NiO–YSZ reduces the CTE difference with the YSZ electrolyte as much as possible, minimizing the internal residual stresses during device fabrication. However, the reduction reaction of the NiO–YSZ precursor structure (during the first cycle of operation) causes drastic changes to the porosity and density of the anode layer and other physical and mechanical properties [2,3,11]. The process introduces a redistribution of stresses in the SOFC component layers, which in turn has major effects on the structural integrity of the SOFC membrane electrolyte assembly (MEA). Internal stresses develop due to the thermal shocks generated by thermal cycling effects during the start-up/shut-down operations of the SOFC [4,6]. Therefore, a detailed study of the mechanical endurance behavior of SOFC components at high operating temperatures and in reactive fuel environments is crucial to solving the reliability issues of MEA, which is susceptible not only to the resultant internal stresses already mentioned but also to assembly stresses and sudden external impacts. Many studies are devoted to the mechanical properties of Ni–YSZ anodes or YSZ electrolytes in the literature. The strength of the YSZ electrolyte and Ni–YSZ anode is evaluated at ambient and elevated temperatures with a concentric ring-on-ring loading configuration [2,7,17–19], and porosity-dependent elastic properties are reported [2–4,11]. Fracture toughness is measured with both indentation fracture and double-torsion loading methods [7,17–19]. However, the ways in which changes in the anode microstructure affect the thermo-mechanical properties of load-bearing anode-electrolyte half-cells is a key issue requiring further attention. It is widely reported that the strength and elastic properties of the NiO–YSZ anode decrease with increasing porosity during the reduction reaction. However, the microstructural development of an anode in a half-cell or positive electrode–electrolyte-negative electrode (PEN) structure is different from the anode sheet due to the presence of the electrolyte (and cathode) on one side. The dense electrolyte prevents gas diffusion from one side, so the development of porosity occurs gradually from the side of the anode that is exposed to the reducing atmosphere. This situation causes a gradient in the porosity and Ni distribution during the reduction process. The distribution of Ni in the YSZ phase is crucial to controlling the CTE of the anode. To fully optimize the anode layer and the anode-electrolyte interface design for anode-supported SOFCs, it is therefore necessary to evaluate the mechanical properties of anode-electrolyte half-cells at elevated temperatures when the chemical stress fields are active.

This paper reports a systematic analysis of the mechanical properties of reduced NiO–8YSZ anode-supported bi-layer SOFC structures at elevated temperatures in ambient air and reducing environments, which was accomplished by simulating the actual operating conditions in SOFCs. Two sets of specimens with different anode thicknesses were studied concurrently to investigate the effects of anode layer thickness on the overall mechanical stability of the SOFC MEA.

2. Experimental procedure

2.1. Sample preparation

The two batches of square-shaped samples (4 in. × 4 in.) of 600- and 900-μm thickness were supplied by Materials and Systems Research, Inc., Salt Lake City, UT, USA. The square laminates of both batches had a dense electrolyte layer (~8-μm thickness) of 8YSZ supported by a thick NiO–8YSZ (70:30 vol.%) anode precursor layer. The anode-electrolyte bi-layer structures were formed by depositing the thin 8YSZ electrolyte layer over the NiO–8YSZ anode layer fabricated by tape casting of powder slurries. The bi-layer structures were co-sintered at approximately 1100 °C for 4 h. The as-received samples were cut into suitable sizes and reduced in a gas mixture of 5% H_2–95% Ar at 800 °C. This reduction was performed in an autoclave setup, in which the samples were pretreated at the aforementioned temperature for 1 h prior to the initiation of the reduction reaction. The gas mixture was introduced in the chamber at a constant flow rate of 3.2 SLPM and the temperature-chemical environment condition was maintained for selected time periods of up to 8 h. The samples were then cooled to room temperature without changing the reducing gaseous environment.

2.2. Sample characterization

The microstructures of the as-received and reduced samples were studied with a JEOL JSM-7000 scanning electron microscope (SEM). An accelerating voltage of 10 kV was used to resolve any microstructural changes in the anode and electrolyte regions or their interface. The porosity in the samples was estimated by the Archimedes principle, as described in ASTM Standard C20-00. The derived values closely approximated the anode's true porosity values because the thickness of the electrolyte layer was negligible compared to that of the anode. The hardness of the samples was measured using the Vickers indentation method, in which a load of 500 g was applied to the anode surfaces for 15 s. Young's modulus of the samples was determined as a function of temperature using an impulse excitation technique with the Buzz-o-sonic software (Buzz Mac, Glendale, WI) by measuring the fundamental vibration frequencies using a customized experimental setup. The equibiaxial strengths of the as-received and reduced samples were determined at room and elevated temperatures in ambient air and reducing atmospheres. A concentric ring-on-ring configuration of alumina was fabricated and used to determine the samples' in-plane biaxial strengths according to ASTM Standard

C1499-05. In this configuration, test specimens with a diameter (D) of approximately 26 mm were spaced concentrically between a loading ring with a diameter (D_L) of 5.5 mm and a supporting ring with a diameter (D_S) of 20 mm. The load was applied to the samples at a constant crosshead displacement rate of 1.2 mm/min, and the equibiaxial strength was calculated using the following equation:

$$\sigma_f = \frac{3F}{2\pi h^2}\left[(1-v)\frac{D_S{}^2 - D_L{}^2}{2D^2} + (1+v)\ln\frac{D_S}{D_L}\right] \quad (1)$$

where F, h, and v are the failure load (N), sample thickness (mm), and Poisson's ratio, respectively. For a rectangular test specimen, the value of D used in Eq. 1 was approximated as

$$D = 0.54(l_1 + l_2) \quad (2)$$

where $l_1$and $l_2$are the lengths of the specimen edges. The edge lengths fell within the range $0.98 \le l_1/l_2 \ge 1.02$. Because the test specimen thickness could not be changed, the values for D_S and D_L were chosen according to the following condition:

$$2 \le \frac{D - D_S}{h} \le 12 \quad (3)$$

The load was applied in the direction of the electrolyte and the anode was kept on the tensile side. Graphite sheets were used as compliant layers. Most of the specimens fractured into three pieces, and the fracture originated within the load ring diameter. The average strength value of at least six specimens was reported, and post-fracture microstructure analysis was performed using SEM to study the fracture-originating flaws.

3. Results and discussion

3.1. Effects of reduction on microstructure development in the NiO–8 YSZ anodes

The SEM micrographs in Fig. 1 show cross-sectional views of the bi-layer structure, illustrating a systematic study of the effects of reduction on microstructure development during the formation of a cermet anode in the 900-μm-thick samples. The as-received NiO–8YSZ anode precursor (Fig. 1a) was relatively dense, with very few irregularly shaped, randomly distributed pores. As the duration of exposure to the reducing atmosphere increased, the NiO gradually reduced to Ni from the edge of the anode side and became fully reduced (confirmed by X-ray diffraction) after 8 h of reduction.

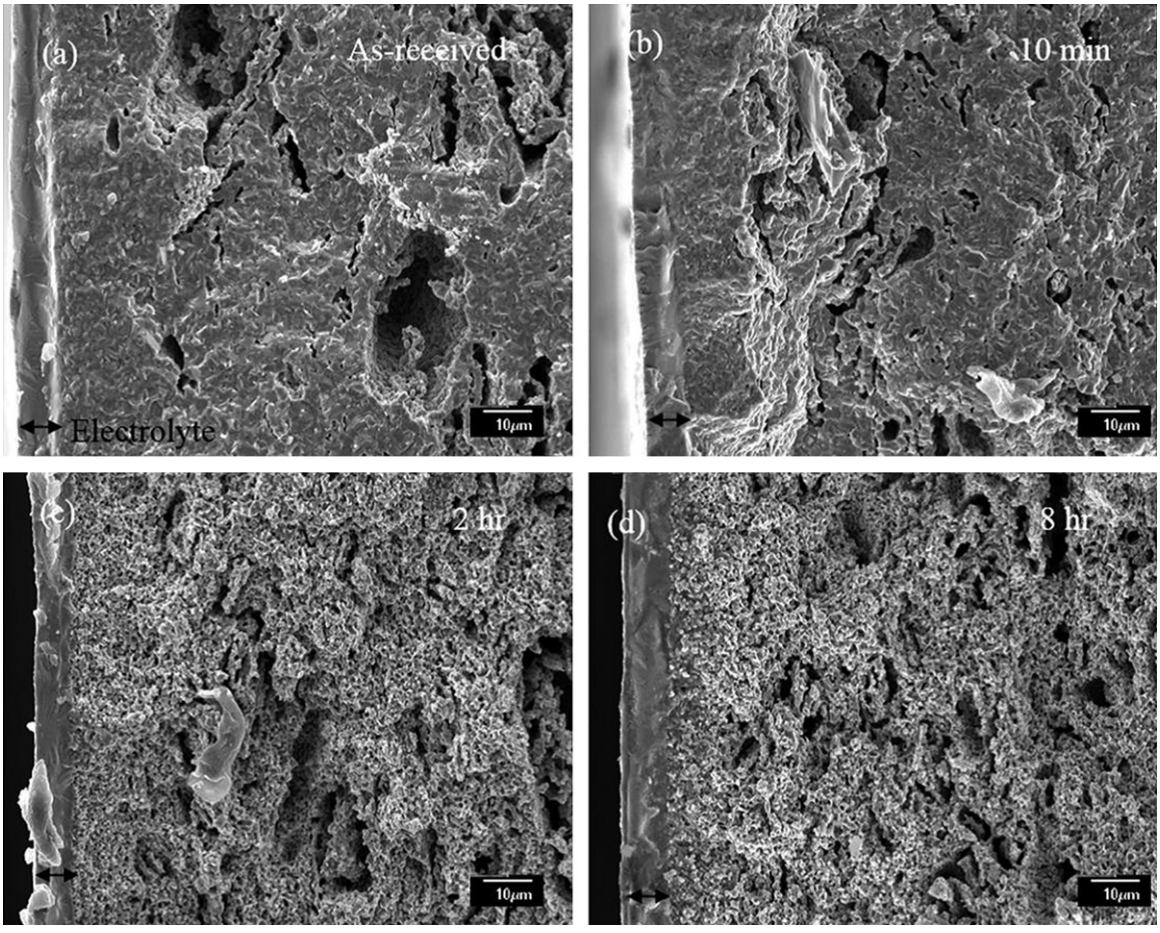

Fig. 1. Effects of reduction on microstructure development in 900-μm-thick NiO–8YSZ half-cells. NiO gradually reduces from the edge of the anode and spreads across the half-cell towards the electrolyte layer as the exposure time increases.

The unreduced portion of the anode closest to the electrolyte after 10 min of reduction is shown in Fig. 1b. Further exposure almost reduced the NiO, as exhibited by the changes to the microstructure in the 2 h and 8 h reduced samples (Fig. 1c and d). The electrolyte remained unaffected, and no delamination of the electrolyte was visible after complete reduction. Fig. 2 shows the microstructural changes in further detail. During the initial stage of reduction, a thin layer of Ni formed on the NiO particles (Fig. 2a and b). Further exposure to the reducing conditions reduced the volume of NiO considerably, which led to the development of a typical porous cermet microstructure with a homogeneous dispersion of Ni particles in 8YSZ and interconnected pores (Fig. 2c). The homogeneous dispersion of electron-conducting Ni with the oxygen conductor 8YSZ dispersed the reaction zones in the volume of the porous electrode. Spreading the reaction zones away from the anode electrolyte interface enhanced the electrochemical conversion rates. The uniformly distributed interconnected pores in the Ni–8YSZ anode provided unbroken percolation paths for electrons, oxide ions, and hydrogen fuel. On the other hand, the required mechanical strength and structural integrity of the anode was maintained by the 8YSZ framework. The high-temperature sintering (1100 °C) of the green anode precursor structure after its deposition resulted in densification and neck formation between the particles in the anode, which was essential to the formation of percolation paths. Therefore, the performance and mechanical stability of the Ni–8YSZ anode depended mainly on the sintering of a well-packed green structure to obtain a mechanically rigid YSZ network capable of restricting the Ni phase from agglomeration during operation. Past studies have reported that the microstructure in Ni–YSZ cermets is highly dependent on the composition, morphology, and synthesis process of the precursor, resulting in significant changes to the overall performance of the SOFC [4,16,20–22]. At least 40 vol% of Ni [23,24] is required for the anode's optimum performance, along with the homogeneous distribution of the Ni and YSZ phases [22]. The Ni phase controls the thermal expansion of the Ni–8YSZ cermet with its high thermal conductivity and plasticity, and leads to high thermal shock resistance [16,25].

3.2. Effects of reduction on the mechanical properties of the NiO–8YSZ anode/8YSZ electrolyte half-cells

Fig. 3a shows the effects of reduction on the equibiaxial strength of the 900-μm-thick half-cells at room temperature in ambient air. The average strength of the as-received half-cells was 275 MPa, which increased suddenly to 399 MPa in the 10 min reduced samples, even though the porosity increased to 18.60% from an initial value of 11.76% in the as-received samples. This change occurred due to the initiation of the formation of a Ni layer on the surface of the NiO grains in the anode. The Ni layer acted as a metallic coating and increased the strength of the half-cells. However, the average strength of the cells started to decrease as the porosity increased further, and reached a value of 290 MPa at a porosity of 23.24% (after 1 h of reduction). After 2 h of reduction, the anode consisted mostly of Ni (with a small

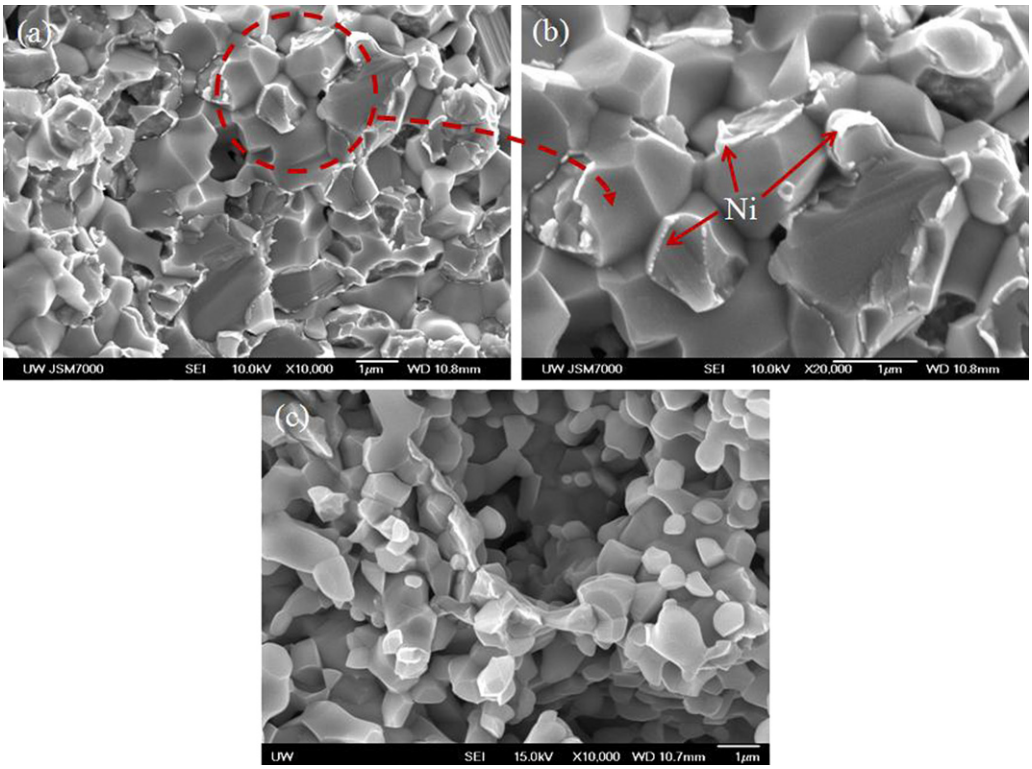

Fig. 2. SEM images detailing the development of the Ni–8YSZ cermet microstructure (900-μm-thick samples): (a) and (b) anode reduced at 800 °C in a 5% H_2–95% Ar environment for 10 min (note the formation of Ni layers on the NiO particles) and (c) fully reduced anodes after 8 h of reduction.

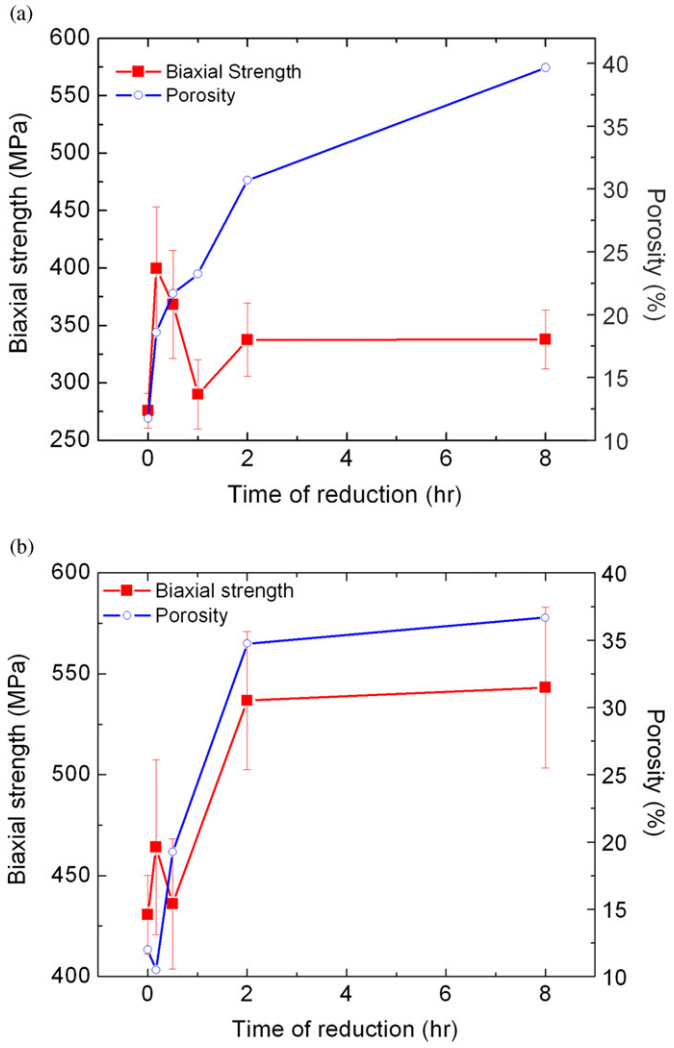

Fig. 3. Effects of reduction on the equibiaxial strength (measured at room temperature in ambient air) and development of porosity in (a) 900-μm- and (b) 600-μm-thick samples.

amount of residual NiO) and the porosity increased to 30.71%. Hence, the half-cells exhibited a steady state in strength values after 2 h of reduction. The scattering in the strength values also reduced with the increase of Ni in the anode structure. The half-cells exhibited a 23% increase in strength after 8 h of reduction, even though the porosity had increased from 11.76% to 39.66%. This increase in porosity had a degrading effect on the strength of the reduced half-cells, but the high metallic Ni content in the anode surpassed the deleterious effects of the porosity and effectively enhanced the specimen's strength after reduction. The 600-μm half-cells showed similar strength behavior with the increase in exposure time to the reducing conditions (Fig. 3b). However, the 600-μm-thick samples were approximately 60.75% stronger after 8 h of reduction than the 900-μm-thick samples. The as-received 600-μm-thick samples had an average strength of 430.64 MPa, which increased to 464.10 MPa after 10 min of reduction and approximately 537 MPa after 2 h of reduction, then remained almost constant thereafter. The porosity increased from 12% to 36.68% (8 h reduced samples) during the reduction process. The fractured surfaces in both sets of samples were analyzed under a SEM to identify the fracture origins. Fig. 4 shows typical SEM micrographs revealing the fracture origins in as-received, partially reduced, and fully reduced samples. The fracture-originating flaws were near-surface volume flaws in most cases, and the fracture origins were either agglomerates of YSZ (Fig. 4a), agglomerates of NiO (Fig. 4b), or cavities formed during casting (Fig. 4c–f). Controlling the volume flaw population generated during anode processing was therefore essential to ensuring higher reliability of the SOFC MEA.

The increase in porosity due to reduction severely affected the hardness of the anode support layer. As shown in Fig. 5, the Vickers hardness value of 5.5 GPa in the as-received 600-μm-thick samples (12% porosity) decreased to less than 1 GPa in the 8 h reduced samples (36.68% porosity). Similarly, the hardness value of 3.13 GPa in the as-received anode layer of the 900-μm-thick samples (11.76% porosity) reduced to approximately 0.40 GPa in the 8 h reduced Ni-8YSZ samples (39.66% porosity). It should be noted that the scattering in hardness values decreased with increasing porosity. Although they were highly porous, the reduced anode samples at 2 h and 8 h had negligible scattering in their hardness values compared to the as-received samples. This type of behavior is attributed to the enhanced plasticity that results from higher Ni metal content in highly reduced porous anodes [3]. The inset in Fig. 5c) shows the effects of heat treatment (in ambient air for 8 h) on the hardness of the 8YSZ electrolytes in the 600-μm-thick half-cells. Because the electrolyte layer remained chemically inert during the heat treatment (and during the reduction process) and had a negligible amount of porosity, it was expected that the hardness would remain independent of indentation load. As shown in Fig. 5c), the heat-treated electrolytes had somewhat consistent hardness values (considering the scattering of these values) at higher loads. The slightly anomalous behavior observed in the low load region was most likely due to the redistribution of stresses in the half-cells caused by heat treatment. The thicker 900-μm samples showed similarly consistent behavior in terms of their electrolyte hardness.

In general, it can be stated that the overall strength and hardness of the half-cells decreased with an increase in the anode support layer's thickness. Although a thicker anode layer enhanced electro-catalytic activities, the decrease in strength and hardness eventually reduced the mechanical stability of the SOFC stack. The electrolyte layer was identical in both sets of samples (~8 μm thick) and the anode porosity was roughly the same in both the as-received and fully reduced samples, so the observed decrease in the thicker samples' overall strength and hardness was essentially due to the increase in anode thickness.

Although the increase in porosity with reduction did not manifest its deleterious effects on the overall strength of the fully reduced half-cells at room temperature, the strength of the samples decreased significantly with the increase in temperature. Table 1 shows the strength of

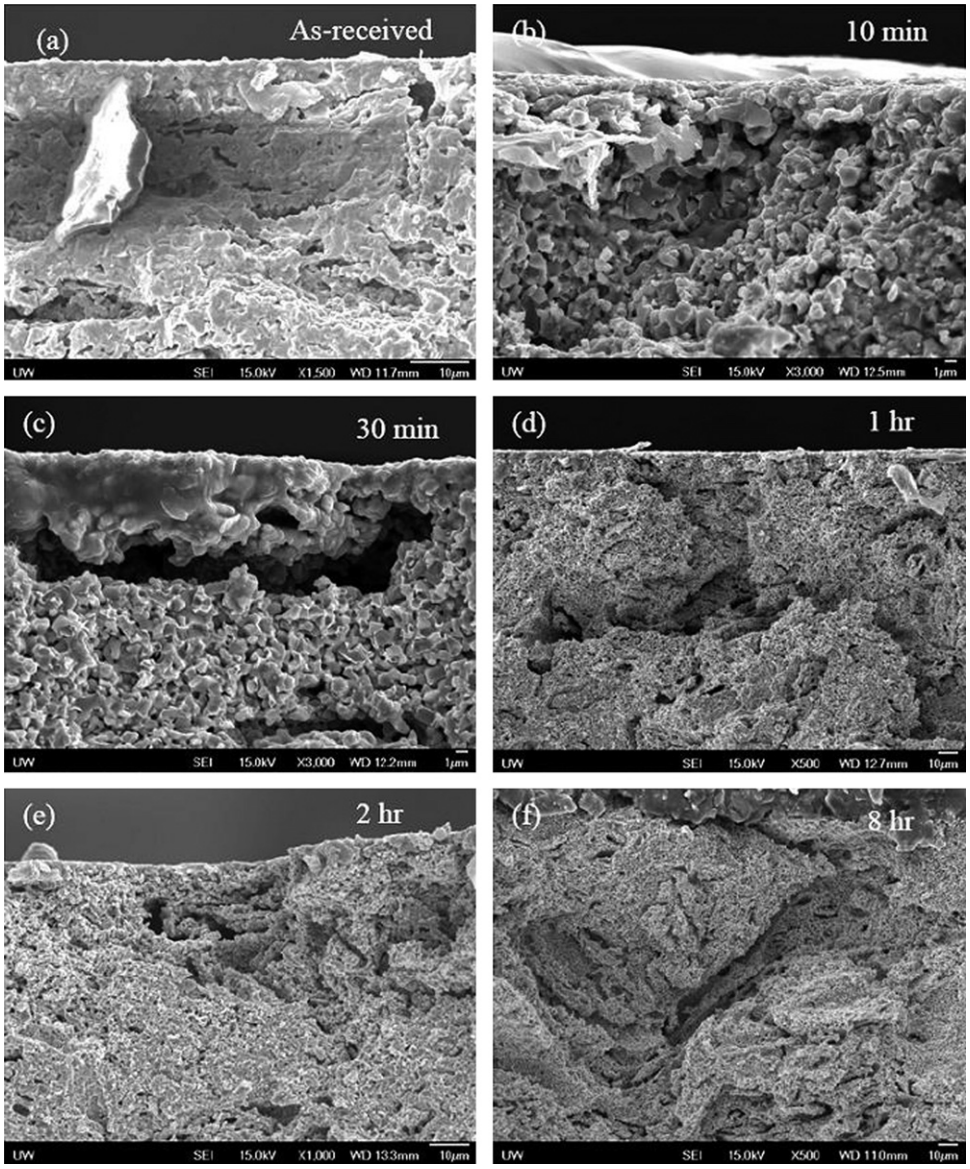

Fig. 4. Typical failure origins closer to the tensile surface (600-μm-thick samples): (a) agglomerates of 8YSZ in as-received samples, (b) pullout of NiO agglomerate in 10 min reduced samples, and (c, d, e, and f) cavities formed during casting in 30- min, 1 hr, 2 h, and 8 h reduced samples.

the as-received and fully reduced half-cells at 800 °C in ambient air and in a 5% H_2–95% Ar environment. Comparison with room-temperature strength values in Fig. 3 clearly indicates a drastic reduction in strength when the as-received samples are evaluated at 800 °C. The strength decreased significantly (by approximately 30–70%) at high temperatures in reducing environments, even in the fully reduced samples. The as-received half-cells displayed catastrophic failure (brittle fracture) during the application of a load at both room temperature and at 800 °C (in air). By contrast, the initial deformation of the fully reduced samples observed during the strength measurements (in 5% H_2–95% Ar environment) was attributable to the Ni's ductile nature. The fully reduced samples eventually failed due to crack growth. As mentioned above, near-surface volume flaws played a critical role in determining the strength of the samples. In addition to intrinsic volume flaws, mostly generated due to the agglomeration of NiO or YSZ particles or cavities formed during the removal of pore-forming organics, the porosity developed during the reduction process also determined the strength of the samples. Furthermore, changes in the elastic properties of the anodes during reduction redistributed the residual stresses in the SOFC. This redistribution may have introduced mismatched stresses in the component layers, which would have a major effect on the structural integrity of the SOFC MEA. Therefore, an assessment of this change in the elastic properties of half-cell samples was needed to optimize the anode design. Fig. 6 shows the temperature dependence of the fully reduced Ni–8YSZ half-cells' Young's moduli for both batches in a 5% H_2–95% Ar atmosphere and compares them with the dependence of the as-received NiO–8YSZ samples' Young's moduli in air in the same temperature

range. The as-received NiO–8YSZ samples, which contained NiO as one of their major constituents (70 vol%), had a characteristically different elastic behavior profile throughout the temperature range (curves *a* and *b*) compared to the reduced Ni–8YSZ cermets, which contained a negligible amount of NiO (curves *c* and *d*). It can be seen that the as-received half-cells (from both batches) had significantly higher Young's moduli at ambient temperature (approximately 118 GPa in 600-μm-thick samples and approximately 108 GPa in 900-μm-thick samples) than the reduced samples due to their lower porosity. Both batches of the as-received samples showed steady room-temperature Young's modulus values up to 150 °C. An increase in the moduli was observed at temperatures over 200–500 °C, with a peak at approximately 325 °C. After this peak, the moduli of the NiO-rich half-cells reduced to steady values as the temperature increased, and remained almost stable until the temperature reached 1000 °C, although considerable modulus scattering was observed at temperatures above 700 °C. The increase in the Young's modulus across the 200–500 °C region is related to the structural transition in NiO from a distorted face-centered rhombohedral to a cubic rock-salt structure near its Neel temperature of 250 °C (antiferromagnetic to paramagnetic transition of NiO) [26,27]. In contrast, the Young's modulus of fully reduced Ni–8YSZ half-cells in a 5% H_2–95% Ar environment shows monotonically decreasing behavior with the increase in temperature. The room-temperature Young's modulus values of the reduced Ni–8YSZ samples were approximately 73 GPa (600-μm-thick samples) and approximately 52 GPa (900-μm-thick samples) in the reducing environment—almost the same as those in ambient air. The 600-μm-thick samples exhibited a sharp decrease in their Young's moduli along the entire temperature range up to 1000 °C, whereas the sharp decrease in the 900-μm-thick samples' Young's moduli values plateaued at 550 °C and remains stable up to 850 °C, and decreasing sharply thereafter until 1000 °C was reached. The total reduction in Young's modulus as the temperature increased from room temperature to 1000 °C in the reducing atmosphere was approximately 44% in the 600-μm-thick samples and approximately 40% in the 900-μm-thick samples. The decrease in Young's modulus with temperatures of up to 600 °C was presumably due to the order-disorder transitions of the oxygen vacancies in the 8YSZ [28,29]. During this transition, the rearrangement of oxygen vacancies and their hopping around active Y cations increased the mechanical losses that resulted in a decrease of the 8YSZ's elastic modulus. This typical behavior of 8YSZ was the reason for the drop in the Young's modulus of Ni-rich, fully reduced

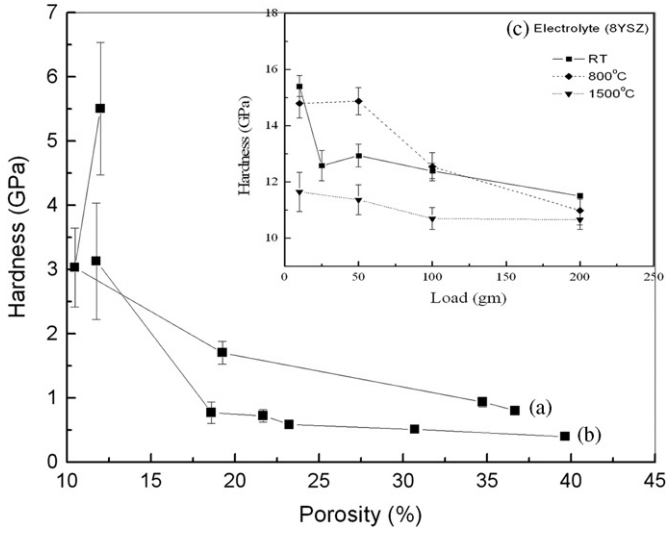

Fig. 5. Hardness values plotted as a function of porosity in the as-received and reduced (a) 600-μm- and (b) 900-μm-thick samples. The inset shows the effect of heat treatment (at 800 and 1500 °C) on the hardness of the electrolyte side of an as-received 600-μm-thick sample.

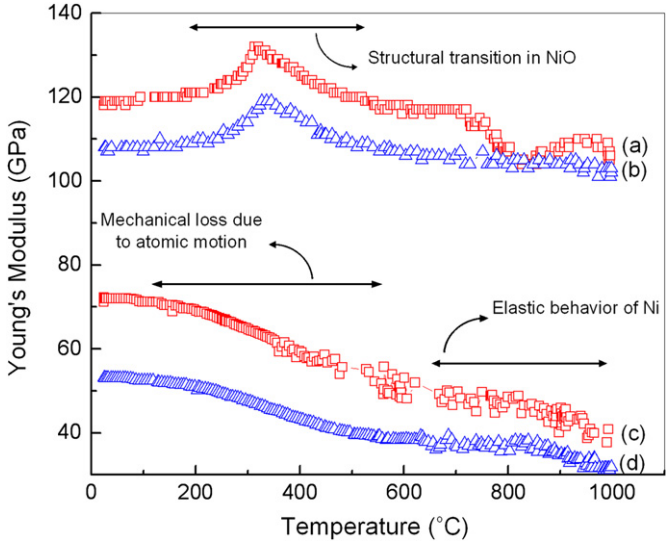

Fig. 6. Variation of the Young's modulus with temperature in (a) and (b) as-received (measured in ambient air) and (c) and (d) 8 h reduced (measured in a 5% H_2–95% Ar environment) NiO–8YSZ 600-μm and 900-μm-thick samples.

Table 1
Equibiaxial strength of the half-cells at 800 °C in ambient air and reducing atmosphere.

Half-cell thickness (μm)	**Strength at 800 °C in air (SD)**[a] (MPa)	**Strength at 800 °C in 5%H_2 (SD)**[b](MPa)
600	217.0 (41.2)	301.4 (31.8)
900	200.5 (5.5)	120.8 (12.2)

[a]As-sintered half-cells.
[b]Fully reduced half-cells. Standard deviation (SD) values are given in parentheses.

half-cells in the 300–600 °C temperature range. These effects were also present in the as-received NiO–8YSZ samples, but the overlapping of effects due to the structural transition in NiO within the 200–500 °C temperature range made them dormant.

The continuous decrease in Young's modulus values with different slopes above 600 °C was essentially related to the elastic properties of Ni at elevated temperatures rather than the 8YSZ. In fact, the Young's modulus of 8YSZ shows a marginal increase at temperatures above 600 °C [30,31].

Based on these results on the mechanical properties of reduced NiO–8YSZ anode-supported bi-layer SOFC structures, a detailed analysis of the distribution of stresses during actual SOFC operation is currently being performed to optimize the SOFC design and predict its reliability.

4. Conclusions

This study developed two sets of bi-layer SOFC half-cell structures with a thin, dense 8YSZ electrolyte layer supported by a thick, highly porous Ni–8YSZ anode by reducing a NiO–8YSZ/8YSZ precursor structure at 800 °C in a 5% H_2–95% Ar environment, and studied these structures to characterize the effects of reduction on their mechanical properties.

The change in equibiaxial strength of the half-cell samples was evaluated as a function of porosity in both ambient air and reducing environments at room and elevated temperatures. The overall strength of the half-cell structures at room temperature increased after reduction, even though the reduced samples became highly porous. It was observed that the 600-μm-thick samples were approximately 60.75% stronger after 8 h of reduction than the 900-μm-thick samples. Although the overall strength of the fully reduced half-cells at room temperature increased after reduction, the strength of the samples significantly decreased with the increase in temperature.

The increased porosity of the reduced anode samples severely affected the hardness and elastic moduli of the samples. The anode hardness decreased drastically after reduction in both sets of samples, and the as-received half-cells of both batches had significantly higher Young's moduli at room temperature than the reduced samples due to their lower porosity. At elevated temperatures, the Ni–8YSZ anodes showed a monotonically decreasing profile in their Young's moduli as a function of temperature, which was significantly different from the behavior of the unreduced NiO–8YSZ samples. As the temperature increased, the Young's modulus of the as-received NiO–8YSZ samples in ambient air peaked over 200–500 °C and then reduced to steady values as the temperature further increased, remaining almost stable until a temperature of 1000 °C was reached. However, Young's modulus values of the fully reduced samples in the reducing environment decreased monotonically with the increase in temperature. Interestingly, the strength, hardness, and elastic properties of half-cell samples with similar compositions and porosities decreased with an increase in the thickness of the anode-supported layer.

Acknowledgments

This work was performed with financial support from the United States Department of Energy Project Grant #DE-FG36-05GO15194. The authors sincerely thank Materials Research and System Inc., Salt Lake City, Utah, USA, for providing the samples.

References

[1] S.M. Haile, Fuel cell materials and components, Acta Materialia 51 (2003) 5981–6000.
[2] M. Radovic, E. Lara-Curzio, Elastic properties of nickel-based anodes for solid oxide fuel cells as a function of the fraction of reduced NiO, Journal of the American Ceramic Society 87 (2004) 2242–2246.
[3] S. Ramanathan, K.P. Krishnakumar, P.K. De, S. Banerjee, Powder dispersion and aqueous tape casting of YSZ–NiO composite, Journal of Materials Science 39 (2004) 3339–3344.
[4] Y. Wang, M.E. Walter, K. Sabolsky, M.M. Seabaugh, Effects of powder sizes and reduction parameters on the strength of Ni–YSZ anodes, Solid State Ionics 177 (2006) 1517–1527.
[5] P.M. Delaforce, J.A. Yeomans, N.C. Filkin, G.J. Wright, R.C. Thomson, Effect of NiO on the phase stability and microstructure of yttria-stabilized zirconia, Journal of the American Ceramic Society 90 (2007) 918–924.
[6] A. Selcuk, A. Atkinson, Elastic properties of ceramic oxides used in solid oxide fuel cells (SOFC), Journal of the European Ceramic Society 17 (1997) 1523–1532.
[7] A. Atkinson, A. Selcuk, Mechanical behavior of ceramic oxygen ion-conducting membranes, Solid State Ionics 134 (2000) 59–66.
[8] A. Selcuk, G. Merere, A. Atkinson, The influence of electrodes on the strength of planar zirconia solid oxide fuel cells, Journal of Materials Science 36 (2001) 1173–1182.
[9] M. Dokiya, SOFC system and technology, Solid State Ionics 152/153 (2002) 383–392.
[10] M. Gaudon, N.H. Menzler, E. Djurado, H.P. Buchkremer, YSZ electrolyte of anode-supported SOFCs prepared from sub micron YSZ powders, Journal of Materials Science 40 (2005) 3735–3743.
[11] S. Primdahl, B.F. Sorensen, M. Mogensen, Effect of nickel oxide/yttria-stabilized zirconia anode precursor sintering temperature on the properties of solid oxide fuel cells, Journal of the American Ceramic Society 83 (2000) 489–494.
[12] S.C. Singhal, Solid oxide fuel cells for stationary, mobile, and military applications, Solid State Ionics 152–153 (2002) 405–410.
[13] T. Setoguchi, K. Okamoto, K. Eguchi, H. Arai, Effects of anode material and fuel on anodic reaction of solid oxide fuel cells, Journal of the Electrochemical Society 139 (1992) 2875–2880.
[14] S.P. Jiang, S.P.S. Badwal, Hydrogen oxidation at the nickel and platinum electrodes on yttria-tetragonal zirconia electrolyte, Journal of the Electrochemical Society 144 (1997) 3777–3784.
[15] S.J. Kim, W. Lee, W.J. Lee, S.D. Park, J.S. Song, Preparation of nanocrystalline nickel oxide-yttria-stabilized zirconia composite powder by solution combustion with ignition of glycine fuel, Journal of Materials Research 16 (2001) 3621–3627.
[16] S.P. Jiang, S.H. Chan, Development of Ni/Y_2O_3–ZrO_2 cermet anodes for solid oxide fuel cells, Materials Science and Technology 20 (2004) 1109–1118.

[17] A. Selcuk, A. Atkinson, Strength and toughness of tape-cast yttria-stabilized zirconia, Journal of the American Ceramic Society 83 (2000) 2029–2035.
[18] M. Radovic, E. Lara-Curzio, Mechanical properties of tape cast nickel-based anode materials for solid oxide fuel cells before and after reduction in hydrogen, Acta Materialia 52 (2004) 5747–5756.
[19] V.A.C. Haanappel, J. Mertens, J. Malzbender, Characterization of Ni-cermets SOFCs with varying anode densities, Journal of Power Sources 171 (2007) 789–792.
[20] M. Brown, S. Primdahl, M. Mogensen, Structure/performance relations for Ni/yttria-stabilized zirconia anodes for solid oxide fuel cells, Journal of the Electrochemical Society 147 (2000) 475–485.
[21] J.H. Lee, J.W. Heo, D.S. Lee, J. Kim, G.H. Kim, H.W. Lee, H.S. Song, J.H. Moon, The impact of anode microstructure on the power generating characteristics of SOFC, Solid State Ionics 158 (2003) 225–232.
[22] W.Z. Zhu, S.C. Deevi, A review on the status of anode materials for solid oxide fuel cells, Materials Science and Engineering A: Structural Materials, Properties, Microstructure and Processing 362 (2003) 228–239.
[23] M. Marinek, K. Zupan, J. Macek, Preparation of Ni–YSZ composite materials for solid oxide fuel cell anodes by the gel-precipitation method, Journal of Power Sources 86 (2000) 383–389.
[24] J.H. Lee, H. Moon, H.W. Lee, J. Kim, J.D. Kim, K.H. Yoon, Quantitative analysis of microstructure and its related electrical property of SOFC anode, Ni–YSZ cermet, Solid State Ionics 148 (2002) 15–26.
[25] M. Mori, T. Yamomoto, H. Itoh, H. Inaba, H. Tagawa, Thermal expansion of nickel–zirconia anodes in solid oxide fuel cells during fabrication and operation, Journal of the Electrochemical Society 145 (1998) 1374–1381.
[26] J. Samuel Smart, S. Greenwald, Crystal structure transitions in antiferromagnetic compounds at the Currie temperature, Physical Review 82 (1951) 113–114.
[27] C.J. Toussaint, A high-temperature X-ray diffraction study of the NiO–Li_2O system, Journal of Applied Crystallography 4 (1971) 293–297.
[28] M. Shimada, K. Matsushita, S. Kuratani, T. Okamoto, M. Koizumi, K. Tsukuma, T. Tsukidate, Temperature dependence of Young's modulus and internal friction in alumina, silicon nitride, and partially stabilized zirconia ceramics, Journal of the American Ceramic Society 67 (1984) C23–C24.
[29] A. Lakki, R. Herzog, M. Weller, H. Schubert, C. Reetz, O. Gorke, M. Kilo, G. Borchardt, Mechanical loss, creep, diffusion and ionic conductivity of ZrO_2–8 mol% Y_2O_3 polycrystals, Journal of the European Ceramic Society 20 (2000) 285–296.
[30] S. Giraud, J. Canel, Young's modulus of some SOFCs materials as a function of temperature, Journal of the European Ceramic Society 28 (2008) 77–83.
[31] M. Radovic, E. Lara-Curzio, R. Trejo, H. Wang, W.D. Porter, Thermophysical properties of YSZ and Ni–YSZ as a function of temperature and porosity, Ceramic Engineering and Science Proceedings 27 (4) (2008) 79–85.